Impact of viscoelasticity on the stiffness of polymer nanocomposites: Insights from experimental and micromechanical model approaches

Jean-Philippe Noyel, Ahmad Hajjar, Rafaela Debastiani, Kevin Antouly, Atilla Atli

Polymer 309 (2024) 127443

Contents lists available at ScienceDirect

Polymer

journal homepage: www.elsevier.com/locate/polymer

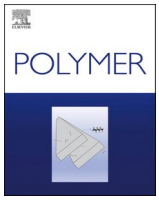

Impact of viscoelasticity on the stiffness of polymer nanocomposites: Insights from experimental and micromechanical model approaches

Jean-Philippe Noyel [a,*], Ahmad Hajjar [b], Rafaela Debastiani [c,d], Kevin Antouly [a], Atilla Atli [a,**]

[a] Univ Lyon, ECAM LaSalle, LabECAM, 69321, Lyon, France
[b] Center for Environmental Intelligence and College of Engineering and Computer Science, Vin University, Ha Noi, Viet Nam
[c] Institute of Nanotechnology (INT), Karlsruhe Institute of Technology (KIT), Kaiserstraße 12, 76131, Karlsruhe, Germany
[d] Karlsruhe Nano Micro Facility (KNMFi), Karlsruhe Institute of Technology (KIT), Hermann-von-Helmholtz-Platz 1, 76344, Eggenstein-Leopoldshafen, Germany

ARTICLE INFO

Keywords:
Viscoelasticity
Nanocomposites
Young's modulus
Micromechanical model

ABSTRACT

The mechanical properties of $BaTiO_3$ filled HDPE nanocomposites are studied by experimental and numerical approaches. First, the viscoelastic behavior of neat HDPE is highlighted experimentally in tensile and relaxation tests. A method is then proposed to define a constitutive viscoelastic law representative of this behavior at different tensile crosshead speeds at room temperature. Afterward, this law is implemented in a finite-element-based micromechanical model representing the $BaTiO_3$ filled HDPE nanocomposites with different filler amounts. The experimental and numerical results are further compared. Both the experiments and numerical simulations confirm the viscoelastic behavior of the polymer nanocomposite. For nanocomposites with filler concentrations up to 20 %, the error between the experimental and numerical findings remains less than 8 %, confirming that the model represents well the composite behavior for low and moderate filler amounts. The proposed strategy can be applied to other polymer composites in order to predict the complete mechanical behavior of viscoelastic composite materials.

1. Introduction

Industries demand more and more performant parts fulfilling simultaneously several tasks. These custom-made parts are often manufactured by multifunctional materials. Composites are one of the promising material families which can satisfy such attempt. However, their development is a scientific challenge since there are several parameters affecting their performance, where the role of each constituent has to be determined. Among these composites, the particulate filled polymer composites are of interest. The final properties of these nanocomposites can be adapted to each application by choosing the appropriate parameters, such as the nature of the parent materials (matrix and particles), their proportions, the shape and the distribution of fillers.

The use of Barium titanate ($BaTiO_3$) filled High Density Polyethylene (HDPE) nanocomposites can meet these requirements. HDPE is one of the largely used thermoplastic polymers by industry due to its simple chemistry, low cost and ease to process. $BaTiO_3$ is frequently employed due to its inherent dielectric/piezoelectric properties [1–4]. Nevertheless, there are a few research on the $BaTiO_3$ filled HDPE nanocomposites and they have mainly focused on the permittivity, electrical and thermal properties [5–9]. Mechanical properties are fundamental characteristics of materials, since they must support mechanical loads during their use. However, there are few investigations on mechanical characterization of $BaTiO_3$ filled HDPE nanocomposites in the literature [7,8,10].

Mechanical properties of composites, and particularly Young's modulus, can be measured experimentally. However, it may be useful to have a predictive model able to calculate these properties as a function of its parent components. These predictive models can be developed using either an analytical or numerical approaches. Analytical approach using a Hashin-Strikman model [11,12] as well as numerical approaches have been employed in several research studies [13–16]. Concerning HDPE filled $BaTiO_3$ nanocomposites, their mechanical properties were studied experimentally and numerically in our recent work [10]. In this investigation, it was attempted to predict the Young's moduli of $BaTiO_3$ filled HDPE nanocomposites with different filler fraction by developing a micromechanical model. The influence of different $BaTiO_3$ particle distribution was underlined. However, the experimental Young's moduli determined from tensile tests have been found different, to some extent,

* Corresponding author.
** Corresponding author.
E-mail addresses: jean-philippe.noyel@ecam.fr (J.-P. Noyel), atilla.atli@ecam.fr (A. Atli).

https://doi.org/10.1016/j.polymer.2024.127443
Received 5 April 2024; Received in revised form 17 July 2024; Accepted 27 July 2024
Available online 28 July 2024

to the ones predicted by the numerical model. Several reasons were proposed to explain the origin of this disparity: shape of the particles considered spherical in the micromechanical model, influence of particle percolation, the modification of polymer properties surrounding filler particles. The later effect i.e. the influence of interphase formed between particles and polymer in polymer composites has been widely studied [17–19]. Another reason of the discrepancy between the experimental and numerical results could be the viscoelastic behavior of polymers. The behavior of HDPE in the micromechanical model developed in this previous work was supposed to be isotropic linear elastic, but the results of tensile tests carried out at different crosshead speeds have clearly shown the influence of strain rate on the measured stiffness, indicating a viscoelastic behavior [10].

The characterization of the viscoelastic behavior of polymer nanocomposites has been the subject of numerous experimental research [20–22]. However, concerning the numerical approach, relatively little work has been done, to the authors' knowledge. For instance, a viscoelastic constitutive law was implemented in a micromechanical model to characterize creep behavior of silica-polyimide nanocomposites [23] or to predict the frequency response of particulate filled polymer [24].

This brief literature review shows that research concerning the mechanical behavior of the $BaTiO_3$-HDPE nanocomposite has been limited to either experimental testing or to numerical modeling assuming linear elastic behavior for the polymer. It also reveals that the mechanical response of the nanocomposite is influenced by the strain rate. In this context, a constitutive model for the polymer, incorporating a time component, is required to better capture the overall mechanical behavior of both neat HDPE and $BaTiO_3$-HDPE composites. Therefore, the aim of the present work is to implement a viscoelastic law in a micromechanical model representing $BaTiO_3$ filled HDPE nanocomposites in order to determine their tensile stiffness for different strain rates. The following approach was used. First, a viscoelastic constitutive law of neat HDPE was defined from experimental tensile and relaxation tests at room temperature for different strain rates. The representativeness of this law was validated by implementing it in a finite element model of neat HDPE and comparing numerical and experimental results. Then, this general constitutive law was implemented into the micromechanical model of $BaTiO_3$ filled HDPE nanocomposites. Finally, numerical results were compared with the experimental ones obtained from tensile tests carried out on this nanocomposite. The approach presented in this paper can be applied to all particulate incorporated polymer nanocomposites.

2. Fundamentals of viscoelasticity

2.1. Viscoelastic behavior

The viscoelastic behavior which is well known on polymers has effects on both short-term and long-term mechanical behavior.

The short-term effects of this viscosity can be seen, for example, on the stress-strain curve in a uniaxial tensile test. Due to viscoelasticity, this curve differs from a straight line: viscoelasticity induces a non-linear behavior. Moreover, the stress-strain curves depend on the strain rate and the temperature. The increase in strain rate leads to an increase in material stiffness; this particular behavior has been highlighted in polyethylene [25,26]. Concerning the effect of temperature, tensile tests on HDPE carried out by Amjadi and Fatemi [27] have shown the influence of temperature and strain rate on Young's modulus and yield stress.

In the long term, the viscoelasticity results in relaxation or creep phenomena. Relaxation refers to the fact that stress decreases in a specimen subjected to constant strain. Conversely, creep refers to the fact that strain increases in a specimen subjected to constant stress. Examples of creep curves for HDPE can be found in Refs. [28,29] and relaxation curves in Ref. [30].

2.2. Constitutive law and characterization methods

For a linear viscoelastic behavior, using the Boltzmann superposition principle, the stress can be expressed from the strain history through the following integral formulation (Equation (1) and [31,32]).

$$\sigma(t) = \int_0^t E_{relax}(t-\tau)\,\dot{\varepsilon}(\tau)\,d\tau \qquad \text{Equation 1}$$

where $E_{relax}(t)$ is the relaxation modulus, and $\dot{\varepsilon}(t) = d\varepsilon(t)/dt$ is the strain rate.

In order to characterize the viscoelastic behavior of materials, the relaxation modulus $E_{relax}(t)$ has to be determined by experimental tests. One of the widely employed experimental approaches to characterize the viscoelastic behavior of a material is in the time domain. In this method, the relaxation modulus $E_{relax}(t)$ can be determined directly from a relaxation test. This method was used for example by Elleuch and Taktak [33] and well suited to characterize the long-term behavior of a viscoelastic material. When we are interested in short-term behavior, as is the case in this work, some corrections must be made at the start of the relaxation phase [34]. This point will be developed and discussed in the next section.

2.3. Viscoelastic models

Two rheological models are commonly proposed to represent the viscoelasticity of polymers: Kelvin and Maxwell models. Kelvin model is generally used to study the creep phenomenon and Maxwell model is applied for relaxation experience [35,36]. In these models, springs and dashpots are used to represent the stiffness and viscous behavior of materials, respectively. A Kelvin element consists of a spring which is in parallel with a dashpot, whereas in Maxwell model, an element contains a spring and a dashpot in series.

A generalized Maxwell model is used in this work to represent the viscoelastic behavior. It contains several Maxwell elements in parallel (Fig. 1).

This model is described by a Prony series representing the relaxation modulus (Equation 2).

$$E_{relax}(t) = E_\infty + \sum_{i=1}^{n} E_i e^{-\frac{t}{\tau_i}} \qquad \text{Equation 2}$$

where E_i is the stiffness of the *ith* component and $\tau_i = \eta_i/E_i$ is its relaxation time, η_i being the viscosity.

3. Materials and methods

The aim of this work is to define a viscoelastic constitutive law of neat HDPE through experiments, and then introduce this law in a micromechanical model of HDPE filled by $BaTiO_3$ nanoparticles.

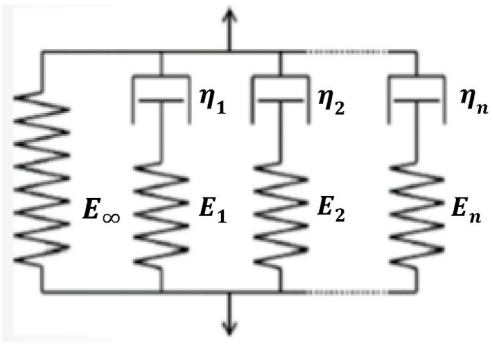

Fig. 1. Generalized Maxwell model.

3.1. Materials

The sample preparation and characterization methods have already been detailed in our previous work [10]. Briefly, the nanocomposite samples were prepared by mixing $BaTiO_3$ nanoparticles (mean size 500 nm) and HDPE in a blender at 170°C–180 °C. In addition to the neat HDPE, the nanocomposite blends with four different $BaTiO_3$ amounts were prepared: 10 v%, 20 v%, 30 v% and 40 v%. Then, the blends were shaped in an injection mold. The thermal, structural and mechanical characterizations of nanocomposites have been performed by Thermogravimetric Analysis (TGA), Differential Scanning Calorimetry (DSC), Fourier Transformed Infrared Spectroscopy (FTIR), X-Ray Diffraction (XRD), Scanning Electron Microscopy (SEM) and tensile tests. The density measurements were done by using a double weighing method and the difference between the theoretical and experimental densities was less than 2 %. This observation would indicate that the composite samples have a homogenous composition and exclude the excessive amount of porosity [10]. In addition to the previously structural characterization, samples extracted from the neat HDPE and the $BaTiO_3$ filled HDPE nanocomposites were scanned using the lab-based nanotomography (nanoCT Xradia 810 Ultra). Through the data reconstruction it is possible to observe the filler particle distribution on the samples as an example for neat, 10v% and 40v% $BaTiO_3$ filled HDPE (Fig. 2). Small samples were cut off with a blade from the tensile test sample and glued in a needle using an UV-curing glue. The nanoCT data was acquired with pixel size of 63.6 nm (sample 40v%) and 127.2 nm (sample neat and 10v%) with acquisition time per projection varying from 20 to 50 s, depending on the sample, and 901 projections were acquired over 180° within a field of view of 65 μm. Neat sample was scanned using Zernike phase contrast mode, while the samples with $BaTiO_3$ particles were characterized using absorption contrast. The nanoCT data was reconstructed using the proprietary software from Zeiss 'Scout and Scan Reconstructor', which is based on the filtered back projection algorithm.

The tensile and relaxation tests are performed by employing a 50 kN Shimadzu AGS-X test machine equipped by a video extensometer, and later compared to the numerical simulations.

A commercial software, *ANSYS 2021R1* is used for the numerical approach.

3.2. From experimental characterization to a viscoelastic model

In this section, the approach used to define a viscoelastic model from experimental data is presented.

It should be noted that the results presented in this section correspond to a single test at a single crosshead speed carried out on a sample of neat HDPE at room temperature. These results are intended to illustrate the method. The overall characterization of the polymer for different crosshead speeds will be detailed in section 3.3.

3.2.1. Experimental characterization

The experimental tensile tests consist of two steps:

a) Step 1 (loading step): a uniaxial load is applied to the sample for a given crosshead speed. The maximum load of 120 N is employed, which corresponds to a normal axial tensile stress around 6 MPa. The maximum tensile stress is assumed to be below to the yield stress of the samples. The time at the end of this step is noted t_1.
b) Step 2 (relaxation step): subsequently the crosshead is held in its position until time t_2. t_2 time has been set to 600 s.

Experimental results are illustrated in Fig. 3. The evolution of strain with time is represented in Fig. 3a. During step 1, the tensile test speed imposed on the crosshead results to a nearly constant strain rate: $\dot{\varepsilon}_1$. A zoom at the beginning of the tensile test is shown in Fig. 3b. During step 2, strain looks like almost constant in time and the strain rate $\dot{\boldsymbol{\varepsilon}}_{\mathbf{2}}$ can be considered as zero. At step 2, a very slight variation of the strain in time appears probably due to sliding of the sample in the grips. The change of stress with time is represented in Fig. 3c. A zoom at the beginning of the relaxation test is shown in Fig. 3d. The effect of viscoelasticity appears in the nonlinear behavior during step 1 and in the relaxation of stress during step 2 as clearly seen on Fig. 3d.

3.2.2. From experimental data to the definition of a relaxation modulus

In a uniaxial tensile test, if the mechanical behavior of the material is perfectly linear elastic, the stress-strain curve is a straight line and the Young's modulus is defined as its slope. For a viscoelastic material like HDPE, the mechanical behavior is nonlinear and the stress strain curve is not a straight line (Fig. 4). Using ISO527-1 Standard, an equivalent Young Modulus is defined as the slope of a straight line between 0.0005 and 0.0025 strain points. It should be noted that this strain range could be used for neat HDPE, but not for HDPE-$BaTiO_3$ nanocomposites which are the main objective of this work. The reason of this inconvenience comes from the fact that $BaTiO_3$ nanocomposites exhibit very small deformation compared to neat HDPE, especially at high $BaTiO_3$ nanocomposites concentrations, such that the resulting strains remain below the strain range used for neat HDPE. In order to focus on the influence of strain rate, as well as the amount of $BaTiO_3$ particles, on mechanical behavior, we determined an equivalent Young Modulus (noted E_{equiv}) defined as the slope of the straight line between 1 and 5 MPa stress

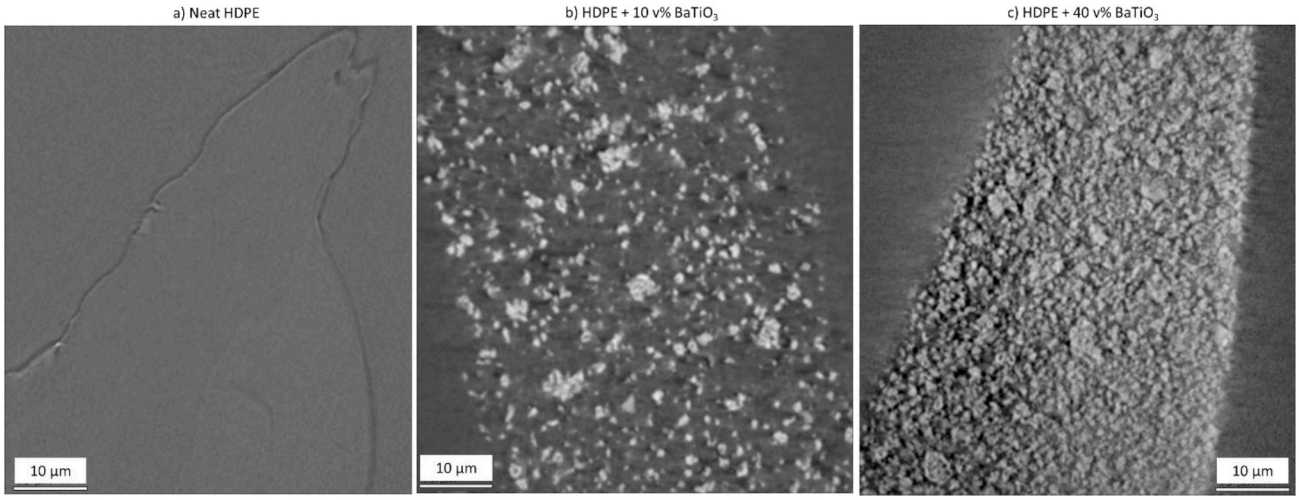

Fig. 2. 2D slices of X-ray nanotomography for the samples: a) neat HDPE, b) HDPE with 10 v% of $BaTiO_3$ and c) HDPE with 40 v% of $BaTiO_3$.

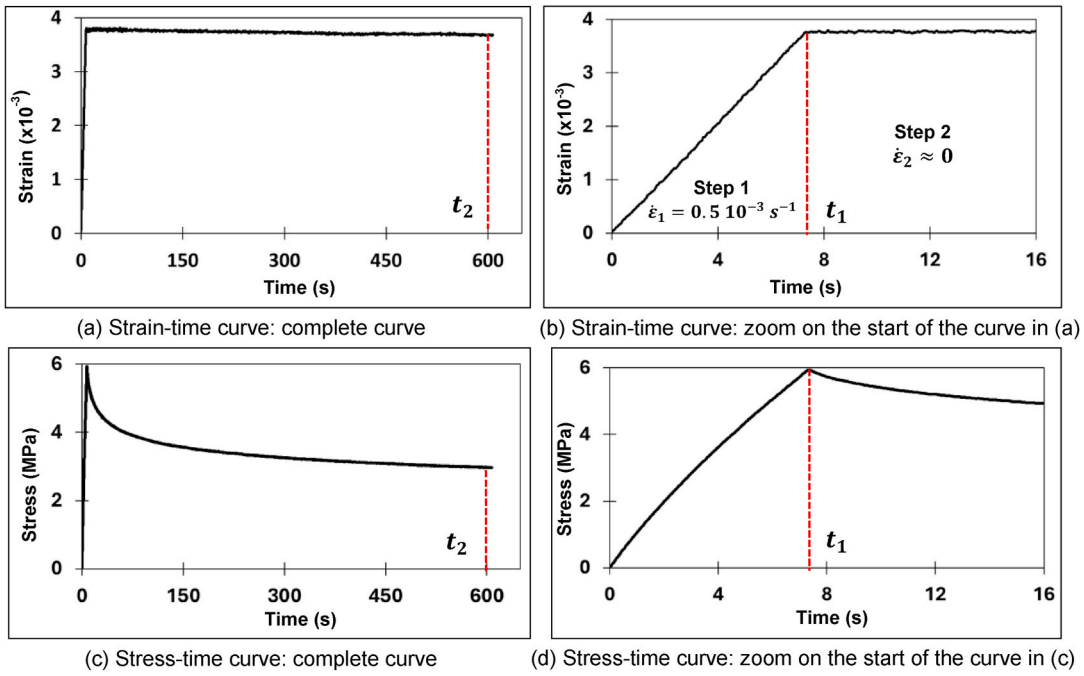

(a) Strain-time curve: complete curve (b) Strain-time curve: zoom on the start of the curve in (a)

(c) Stress-time curve: complete curve (d) Stress-time curve: zoom on the start of the curve in (c)

Fig. 3. Tensile and relaxation tests on neat HDPE sample.

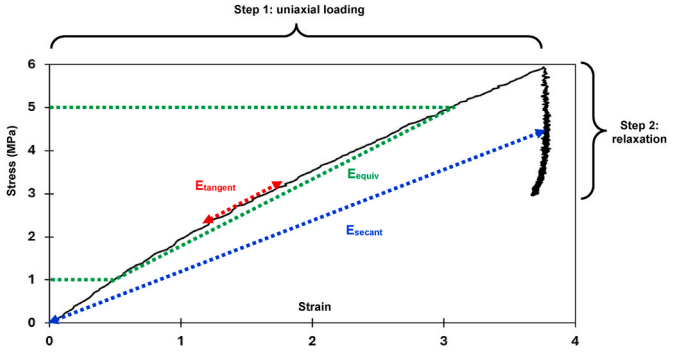

Fig. 4. Experimental stress-strain curve (black line) and definition of Young's moduli.

points (Fig. 4 and Equation (3)) on stress-strain curves. $\varepsilon_{\sigma=5\ MPa}$ and $\varepsilon_{\sigma=1\ MPa}$ are the strains corresponding to 1 MPa and 5 MPa stress points.

$$E_{equiv} = \frac{5\ MPa - 1 MPa}{\varepsilon_{\sigma=5\ MPa} - \varepsilon_{\sigma=1\ MPa}} \quad \text{Equation 3}$$

This definition of E_{equiv} is based on stress rather than strain, in order to avoid the aforementioned problem of the low strains encountered with $BaTiO_3$ filled composites. In addition, the values of stress (1 and 5 MPa) are selected specifically to encompass most of the loading phase.

The viscoelastic behavior is defined by the relaxation modulus $E_{relax}(t)$ (Equation (1)). This relaxation modulus is usually determined from a relaxation test, but it can also be extracted from a uniaxial loading stress-strain curve as follows.

During the loading step, the relaxation modulus corresponds to the tangent modulus (Equation (4)) which is the slope of the stress-strain curve (Fig. 4) [37].

$$E_{tangent}(t) = \frac{d\sigma(t)}{d\varepsilon(t)} \quad \text{Equation 4}$$

During the relaxation step, the secant modulus (Fig. 4) should be used as the relaxation modulus $E_{relax}(t)$ (Equation (5))

$$E_{secant}(t) = \frac{\sigma(t)}{\varepsilon(t)} \quad \text{Equation 5}$$

However, the secant modulus corresponds strictly to the relaxation modulus only in the ideal case where the load is applied suddenly [37, 38]. If the load is not applied instantaneously, which is the real case, the secant modulus differs from the relaxation modulus for the short time of the relaxation step. This point will be illustrated and discussed later.

During the relaxation step, the numerical value of the secant modulus can be determined directly from the stress and strain measured for each time step. However, the numerical value of the tangent modulus cannot be evaluated directly from experimental data due to the noises in stress and strain measurements, since a small variation in stress or strain can result in a big change in derivative. In order to transform an experimental noisy curve, the stress-strain curve is first fitted with a high degree polynomial. Then the tangent modulus is computed from the high degree polynomial approximation of experimental curves $\boldsymbol{\sigma}(\boldsymbol{t})$ and $\boldsymbol{\varepsilon}(\boldsymbol{t})$. An example of relaxation modulus determined from tests on neat HDPE is given in Fig. 5.

A discontinuity is observed between the two steps at instant t_1, due to the way of calculation of E_{relax}. In particular, this discontinuity arises because the relaxation modulus would correspond to the secant modulus of step 2 only if the load were applied suddenly, which is not the case here.

3.2.3. *From relaxation modulus to viscoelastic model*

The curve fitting tool included in the commercial software ANSYS is used to determine the parameters of Prony series from experimental relaxation modulus $E_{relax}(t)$. Some points are extracted from the experimental curve to achieve the curve fitting calculations. In order to highlight the influence of the point selection for curve fitting, two models (Model1 and Model2) are computed from two different sets of experimental points (Fig. 6). In Model1, the points are selected close to t_1 in loading step and far from t_1 in the relaxation step, while in Model2, the selected points are far from t_1 in loading step and closer to t_1 in relaxation step.

In order to represent the evolution of the relaxation modulus as accurately as possible over the whole duration of experiments, a

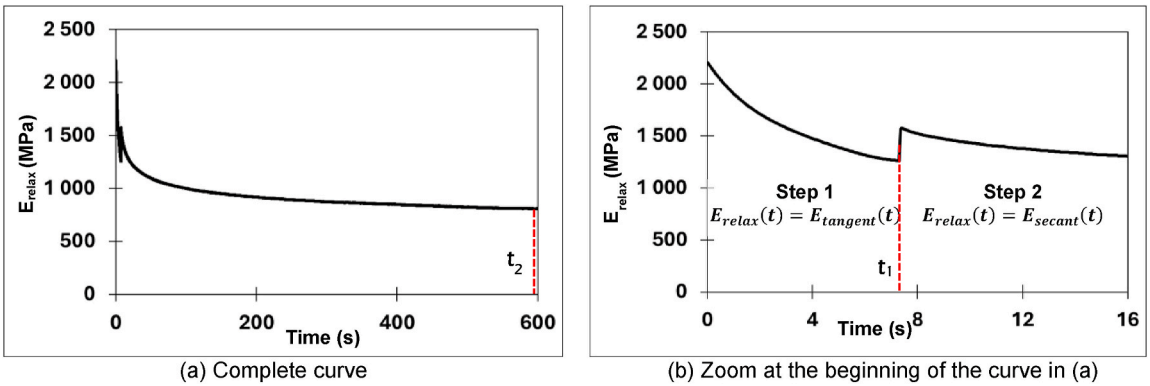

(a) Complete curve (b) Zoom at the beginning of the curve in (a)

Fig. 5. Relaxation modulus determined from experimental stress-strain curve on neat HDPE.

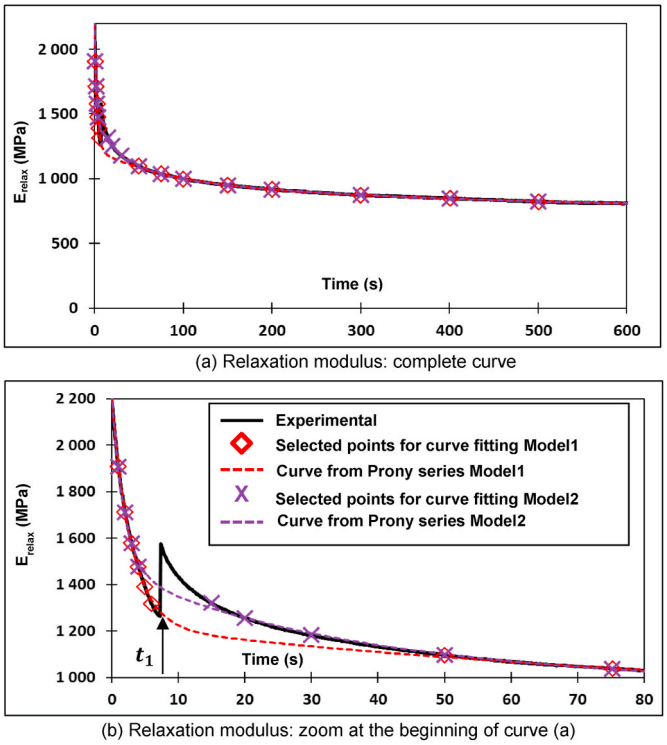

(a) Relaxation modulus: complete curve

(b) Relaxation modulus: zoom at the beginning of curve (a)

Fig. 6. Experimental relaxation modulus with the points selected for curve fitting with two different models.

generalized Maxwell model with three terms in Prony series (Equation 2) is used. The parameters extracted by using curve fitting tool in ANSYS are listed in Table 1.

The relaxation modulus computed (Equation 2) with these parameters (Table 1) is also represented in Fig. 6 for two models (dotted curves). It is clear that the relaxation modulus calculated from these two models corresponds well to experimental points selected for curve fitting.

Table 1
The parameters of Prony series obtained by curve fitting for two models.

i	Model1		Model2	
	E_i (MPa)	τ_i (s)	E_i (MPa)	τ_i (s)
∞	583	/	735	/
1	979	2.96	891	2.48
2	290	88.8	317	53.6
3	352	1316	270	453

3.2.4. *Validation: numerical simulation of the tensile test*

In order to validate these models and quantify the influence of point selection for curve fitting, these models are then implemented in a 2D plane stress finite element model corresponding to the experimental tests. As an example, a neat HDPE sample studied experimentally is shown in Fig. 7a. The geometry of the numerical model is a rectangular surface (Fig. 7b) representing the central part of the sample in Fig. 7a. A displacement δ is applied during a first load step (Fig. 7c), then kept constant during a second one (Fig. 7d). The value of the imposed displacement δ is chosen so that the experimentally measured strain at the end of the loading step is obtained.

Numerical stress computed with these two models are compared to the experimental results (solid black curve) in Fig. 8a. It is remarked that

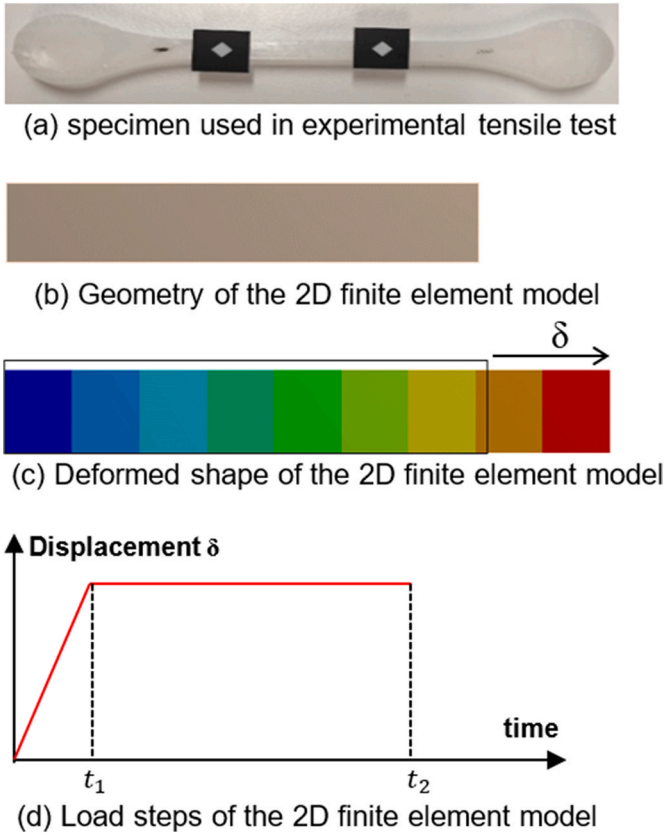

(a) specimen used in experimental tensile test

(b) Geometry of the 2D finite element model

(c) Deformed shape of the 2D finite element model

(d) Load steps of the 2D finite element model

Fig. 7. Numerical approach for neat HDPE. Experimental tensile test specimen of neat HDPE (a), 2D finite element model (b), deformation of the sample under load (c) and applied displacement in two steps (tensile and relaxation) loading (d).

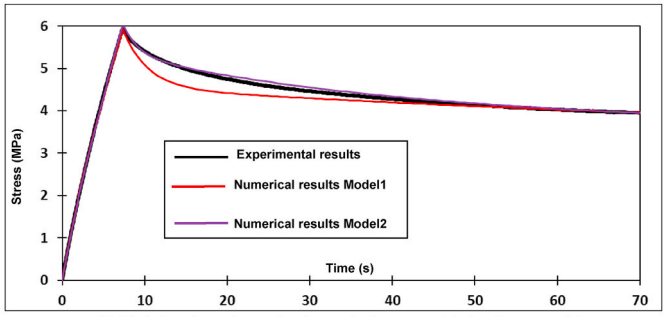

(a) Evolution of experimental and numerical stresses with time for two models

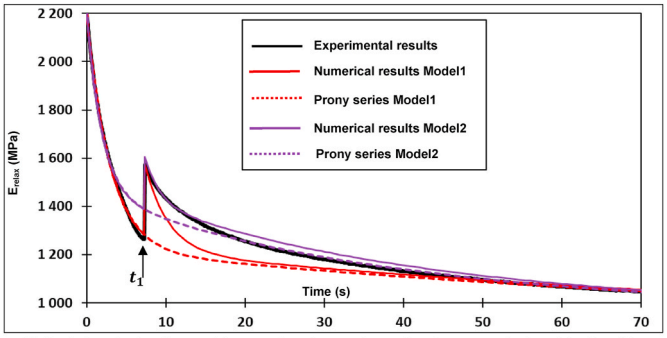

(b) Evolution of relaxation modulus over time for experimental and two numerical models plotted by using the parameters of two Prony series

Fig. 8. Comparison of the experimental and numerical results for two models.

Model2 gives a better correlation with experimental data at the start of the relaxation step.

A tangent modulus (loading step) and a secant modulus (relaxation step) can also be computed from these numerical results, in the same way as they were determined from experimental data. Fig. 8b provides a comparison of the various relaxation moduli calculated from numerical results of the two models (solid red and purple lines), experiments (solid black line), and Prony series-based theoretical results for the two models (dotted curves). These outcomes confirm that the relaxation modulus defined by the Prony series is equal to the tangent modulus during the loading step and to the secant modulus during relaxation step, except for the short time at the beginning of the relaxation step.

The choice of points used for the curve fitting of Model1 results from this property: during the first step, the tangent modulus is strictly equal to the relaxation modulus and curve fitting points are selected along the entire curve up to time t_1; the first point of the relaxation step is then chosen so that a decreasing modulus over time is obtained. The stress calculated with this model corresponds perfectly to that measured during the loading step but shows a slight difference at the start of the relaxation step (just after t_1).

To obtain a better correlation at the start of the relaxation step, a second model was calculated using a new set of curve fitting points. For the relaxation step, the points closer to time t_1 were added, which led to remove the last points close to t_1 in step 1 in order to maintain a decreasing modulus (Fig. 6b). Concerning the correlation between numerical and experimental stresses, this second model results in an improvement during step 2 without an important influence during step 1. The stress is less dependent on the relaxation modulus during the loading step than during the relaxation step, since during the loading step, the relaxation modulus is determined from the derivative of stress i.e. $d\sigma(t)/d\varepsilon(t)$ (Equation (4)), whereas during the relaxation step, it is directly proportional to the stress i.e. $\sigma(t)/\varepsilon(t)$ (Equation (5)). It is therefore more difficult to determine the tangent modulus accurately: a small change in the measurements can result in a large change in its derivative.

To conclude, the approach described in this section was successfully validated: the relaxation modulus determined from the experimental data (tangent modulus for the loading step, secant modulus for the relaxation step) can then be used to describe an effective representative model for viscoelastic behavior of HDPE. Since Model2 led to a better overall correlation, the points at the transition zone between two steps around time t_1 were excluded for curve fitting.

3.3. Overall approach

The method used to define a viscoelastic model from an experimental characterization was described in the previous section, at a fixed crosshead speed. The aim of the work presented in this paper is to introduce a viscoelastic behavior of HDPE into a micromechanical model of $BaTiO_3$ filled HDPE nanocomposites representative of the behavior of HDPE at all strain rates. The overall approach used to meet this objective is illustrated in Fig. 9.

The first step (Fig. 9a and b) concerns the experimental mechanical characterization of neat HDPE and $BaTiO_3$ incorporated HDPE nanocomposites (0 v%, 10 v%, 20 v%, 30 v% and 40 v% in $BaTiO_3$). All tests were performed at room temperature. For each material i.e., 0 v%, 10 v%, 20 v%, 30 v% and 40 v% $BaTiO_3$ filled HDPE, three different samples were characterized at different tensile crosshead speeds, and for each speed, the test was repeated thrice. Finally, an average curve was computed from these nine experimental curves for each speed. An example is given in Fig. 10 for a tensile crosshead speed of 1 mm/min on neat HDPE. The equivalent Young Modulus $\boldsymbol{E_{equiv}}$ defined in Equation (3) is then extracted from the average stress strain curve $\boldsymbol{\sigma(\varepsilon)}$. For neat HDPE, an average relaxation modulus $\boldsymbol{E_{relax}(t)}$ is also computed for each speed.

The second step (Fig. 9c) consists of defining a viscoelastic model representative of neat HDPE which takes into account all crosshead speeds. To do so, an average relaxation modulus is calculated from the various relaxation moduli obtained for each speed. A viscoelastic model is then defined from this global average relaxation modulus, as explained in the previous section.

In order to estimate the correctness of this generalized viscoelastic model to effectively represent the behavior of neat HDPE, numerical stress strain curves $\boldsymbol{\sigma(\varepsilon)}$ and equivalent Young's modulus ($\boldsymbol{E_{equiv}}$) are computed with this model (Fig. 9c) and compared to the experimental results (Fig. 9d).

Finally, the generalized viscoelastic model obtained on neat HDPE is applied to the micromechanical model on $BaTiO_3$ filled HDPE nanocomposites (Fig. 9e), and numerical results are compared with experimental results for different crosshead speeds. This strategy can be justified, since the viscosity is mainly induced by polymer rather than the ceramic fillers.

4. Results and discussion

4.1. Neat HDPE: characterization and definition of a general viscoelastic model

4.1.1. Characterization of the relaxation modulus

Using the approach described in the previous section, experimental relaxation modulus $\boldsymbol{E_{relax}(t)}$ is evaluated for the following crosshead speeds: 0.5, 1, 2, 5, 10, 50 and 100 mm/min. The results are presented in Fig. 11.

The modulus determined in the relaxation step is almost independent of the crosshead speed used in the loading step. The dispersion of the different curves is greater for $\boldsymbol{E_{relax}(t)}$ determined from the tangent modulus of the loading step. For relatively fast crosshead speeds i.e. 50 and 100 mm/min, only the relaxation step is considered. In fact, during the loading step, load is applied very fast which makes it difficult to determine accurately the slope.

4.1.2. Viscoelastic model for neat HDPE

In order to select a set of points for curve fitting, an average relax-

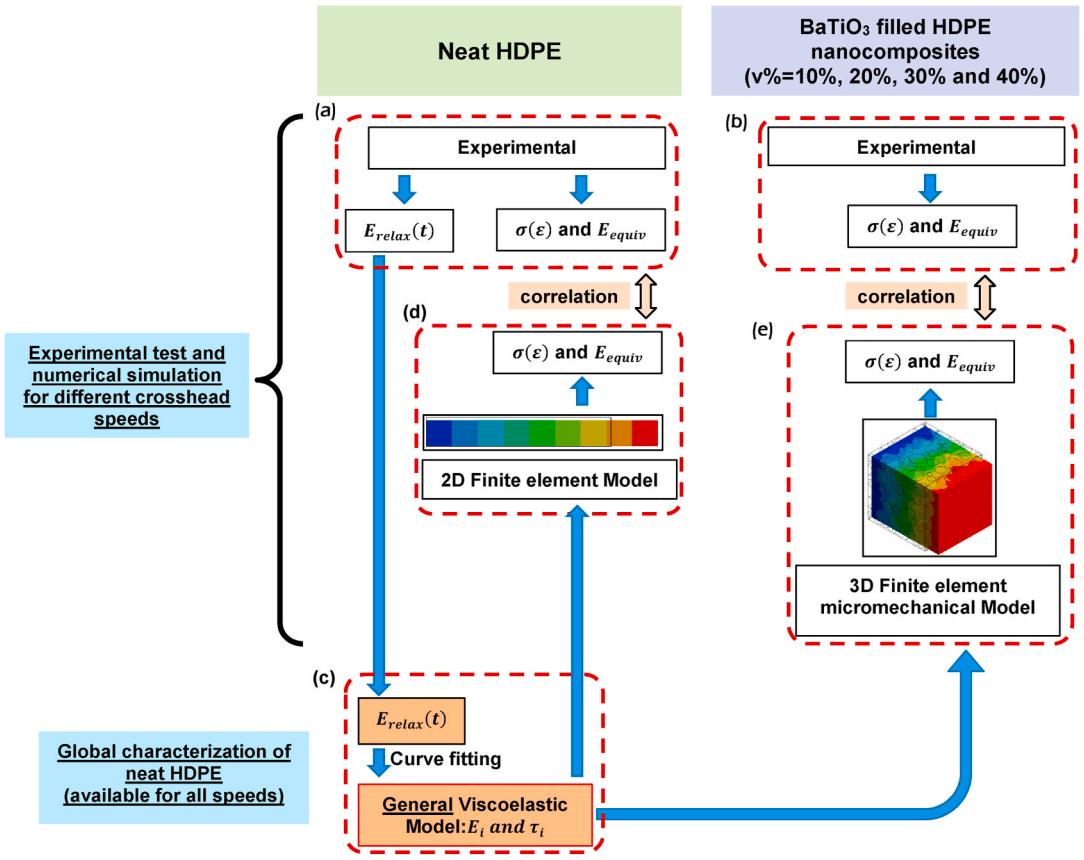

Fig. 9. Approach used to define and validate a viscoelastic model (a), (c) and (d) on neat HDPE (b) and (e) on $BaTiO_3$ filled HDPE nanocomposites.

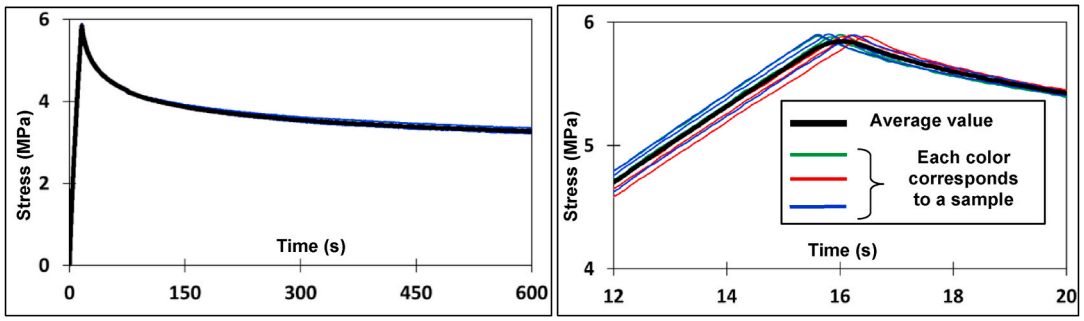

(a) Complete curve (b) Zoom at the beginning of experiments

Fig. 10. Example of an average curve obtained from nine stress-time curves with a 1 mm/min crosshead speed on neat HDPE (each color (blue, green and red) corresponds to a sample and three tests are performed on each sample). (For interpretation of the references to color in this figure legend, the reader is referred to the Web version of this article.)

ation modulus curve is calculated from the curves obtained for different crosshead speeds. It should be noted that for each speed, values just before and just after time t_1 are excluded from the calculation of the average value, in the same way as the points used to define Model2 (Fig. 6). The set of points selected on the average curve for curve fitting are represented in Fig. 11: the whole experimental span (Fig. 11a) and at the beginning of the experiments (Fig. 11b).

The parameters of the Prony series resulting from the curve fitting process in ANSYS are given on Table 2. The relaxation modulus curve plotted by using these Prony parameters are also represented in Fig. 11 (thick black curve).

4.1.3. Validation of the model on neat HDPE

In order to check the viscoelastic final model previously defined (Table 2) representing the behavior of the neat HDPE, the numerical approach defined in Fig. 7 is used for the four lowest crosshead speeds (0.1, 1, 2 and 5 mm/min).

The change of stress with time for experimental results and numerical calculations is illustrated for different crosshead speeds in Fig. 12. The curves over entire experimental time span are presented in Fig. 12a, and the initial parts of these curves are shown in Fig. 12b. The continuous lines are the experimental curves with different crosshead speeds and the dotted lines are the numerical ones obtained from the general viscoelastic model by using the Prony parameters in Table 2. A very good agreement is observed between numerical results and experimental data for these crosshead speed on neat HDPE.

The experimental and numerical stress-strain curves are then plotted (Fig. 12c). The average strain rate corresponding to each crosshead

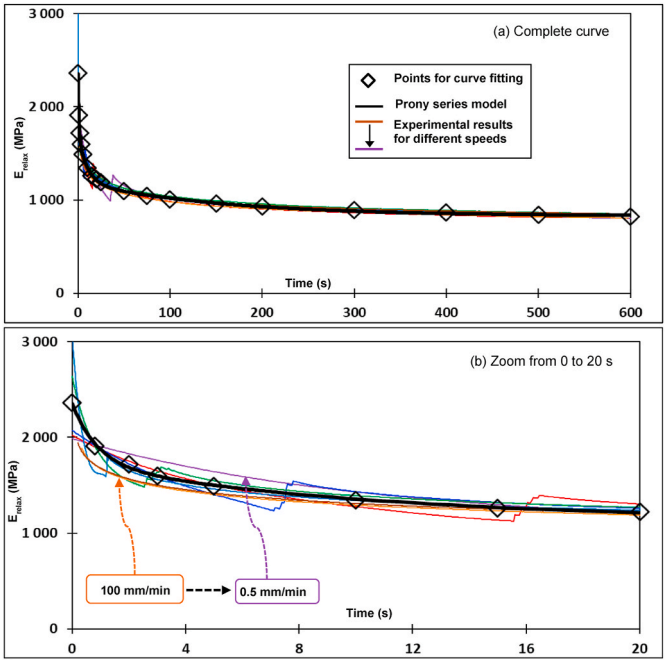

Fig. 11. Relaxation modulus for different crosshead speeds (continuous lines) and set of points (⋄) used for curve fitting (a) the whole experimental span, (b) zoom at the beginning of experiments. The thick black curve is the relaxation modulus plotted by using the Prony parameters in Table 2.

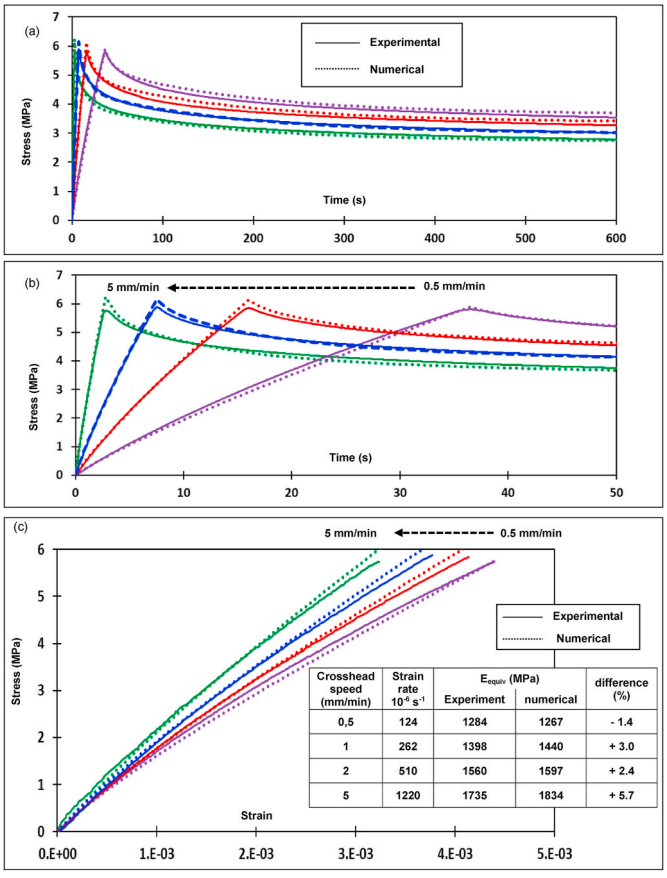

Fig. 12. Experimental (continous lines) and numerical (dotted lines) results for different crosshead speeds on neat HDPE: stress-time curves over the entire time span (a), zoom at the beginning (b) and stress - strain curves (c).

speed and the equivalent Young's moduli are summarized in the table in the inset of Fig. 12c.

These curves clearly confirm the viscoelastic behavior of HDPE: stress-strain curves are not straight lines, and the stiffness depends on the loading speed. In fact, when the crosshead speed increases, the equivalent Young's modulus increases. We also remark that the strain rate is almost directly proportional to the crosshead speed.

A good agreement is observed between experimental and numerical results. The difference between numerical and experimental Young's moduli seems to increase with increasing crosshead speed but still remains negligible. To conclude, the model proposed previously represents well the viscoelastic behavior of neat HDPE.

4.2. *$BaTiO_3$ filled HDPE nanocomposites: characterization and micromechanical modeling*

The viscoelastic constitutive law of neat HDPE is then implemented into a micromechanical model for determining the behavior of $BaTiO_3$ filled HDPE nanocomposites. Numerical results obtained using this law are compared with experimental results.

The experimental approach described in the previous section is applied to the nanocomposite samples, but only the first step, i.e., loading step, was performed. Samples with different amount of $BaTiO_3$ filler are tested: 10 v%, 20 v%, 30 v% and 40 v%. The tests were performed using the following crosshead speeds: 0.5, 1, 2 and 5 mm/min. As for neat HDPE, three different samples are tested for each crosshead speed and the test is repeated at least thrice on each sample for a given speed. Finally, an average curve is computed and plotted.

4.2.1. *Micromechanical model*

The *Material Designer* application of ANSYS is used to generate a 3D geometry of the Representative Volume Element (RVE) of nanocomposites. The distribution of $BaTiO_3$ particles (considered spherical) is chosen as random with a mean particle diameter of 0.5 μm and a standard deviation of 0.15 μm, as determined by using SEM in our previous work [10]. The random particle distribution for the amounts of 10 v% and 40 v% are shown as examples in Fig. 13a and b, respectively. For random particle distribution, the size of this RVE must be large enough that the macroscopic results should be independent of particle distribution. For each amount of $BaTiO_3$ filler, the RVE size was adjusted in a way that the standard deviation of macroscopic Young's modulus with 10 different random distributions remains less than 1 %. A more detailed description of the creation of the RVE can be found in Ref. [10].

This geometry of the RVE is then transferred in the *Mechanical* application tool (finite element software) of ANSYS. The Boundary Conditions (BC) representing a macroscopic uniaxial test are applied. A displacement δx is imposed in x direction and displacements in y (δy) and z (δz) directions are let free but imposed constant (Fig. 13c).

The macroscopic normal strain is defined from the imposed displacement (Equation (6)), and macroscopic normal stress is computed from reaction force (Equation (7)).

$$\varepsilon_{macro}(t) = \frac{\delta_x(t)}{a} \qquad \text{Equation 6}$$

$$\sigma_{macro}(t) = \frac{F_x(t)}{a^2} \qquad \text{Equation 7}$$

where $\varepsilon_{macro}(t)$, $\delta_x(t)$, a, $\sigma_{macro}(t)$, $F_x(t)$ are the macroscopic strain, the imposed displacement in x direction, the length of cube edge of RVE, macroscopic normal stress and applied force in x direction, respectively.

For each amount of $BaTiO_3$ filler and each crosshead speed, the imposed displacement $\delta_x(t)$ is calculated so that the macroscopic strain corresponds to the experimentally measured strain.

The material properties used for the calculations are shown in Table 3. The mechanical behavior of HDPE is simulated by the viscoelastic model found in the previous sections. $BaTiO_3$ particles are

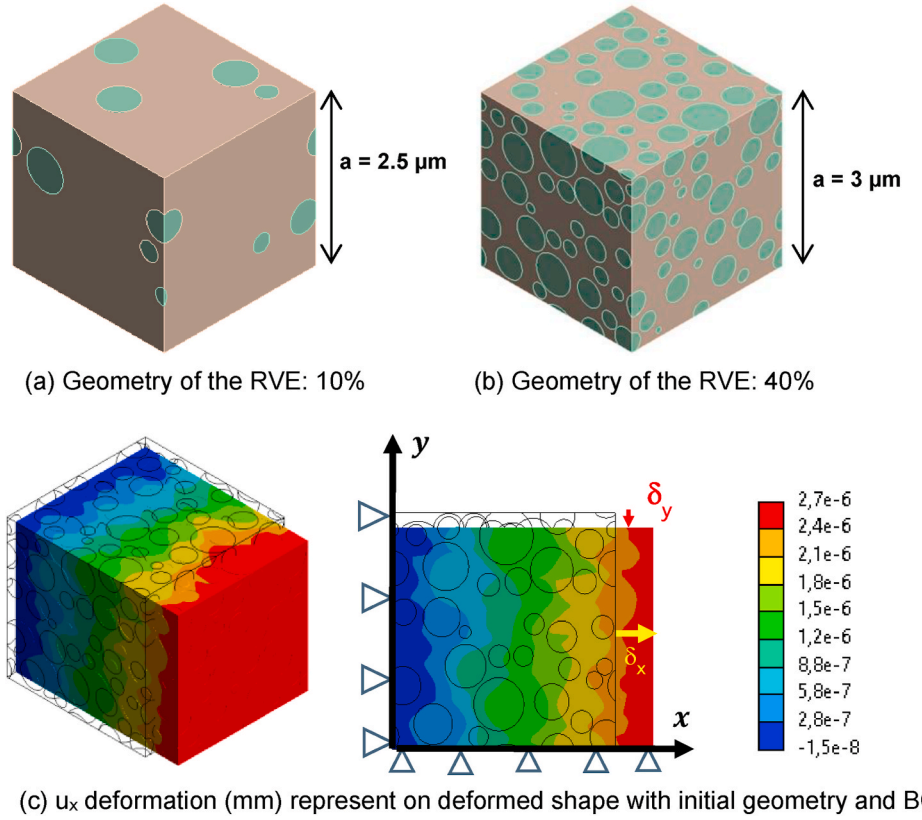

Fig. 13. RVE of randomly distributed $BaTiO_3$ particles in HDPE matrix with different filler amount (a) 10 v%, (b) 40 v%, (c) boundary conditions and results for 40 v % filler when a uniaxial displacement (δx) is applied in x direction.

Table 2
Prony series parameters final model.

	E_i (MPa)	τ_i (s)
∞	827	/
1	626	0.887
2	538	9.59
3	363	156

Table 3
Material properties of HDPE matrix and $BaTiO_3$ filler used in the micro-mechanical model.

Material		
$BaTiO_3$ particles	Isotropic elasticity	
	Young's modulus: 200000 MPa	Poisson's ratio (ν): 0.3
HDPE polymer matrix	Viscoelastic model defined in Table 2	

supposed to have a linear elastic isotropic behavior.

4.2.2. Results

The experimental and numerical stress-strain curves are obtained for each composition of nanocomposites with different crosshead speed. As an example, the experimental stress-strain curves (continuous lines) and numerical (dotted lines) ones are illustrated for 20 v% $BaTiO_3$-filled HDPE composite (Fig. 14a) for different crosshead speeds.

As for neat HDPE, the viscoelastic behavior clearly appears for nanocomposites: an increase in the tensile crosshead speed leads to an increase in the stiffness of the nanocomposites. The equivalent Young's Modulus strongly depends on the strain rate as summarized on the table of the inset on Fig. 14a.

The experimental and numerical results for all filler amounts and all

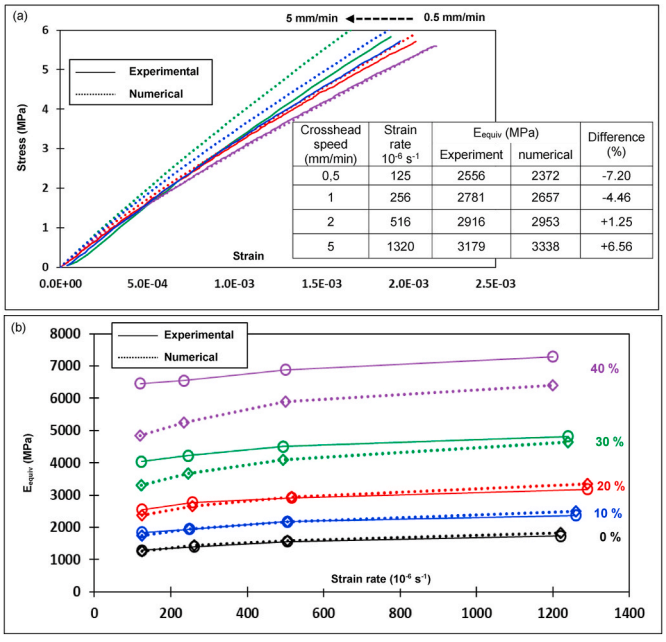

Fig. 14. Experimental (continuous lines) and numerical (dotted lines) results for $BaTiO_3$ filled HDPE stress-strain curves for HDPE filled by 20 v% $BaTiO_3$ with different tensile crosshead speeds (a) equivalent Young's moduli against strain rate for all the HDPE-$BaTiO_3$ nanocomposite samples (b).

crosshead speeds are summarized on Table 4 and represented in Fig. 14b. Fig. 14b shows the evolution of the experimental (continuous lines) and numerical (dotted lines) equivalent Young's moduli as a

Table 4
The experimental and numerical equivalent Young's moduli for all the samples and all crosshead speeds.

Amount of $BaTiO_3$ filler (v %)	Crosshead speed (mm/min)	Strain rate (10^{-6} s^{-1})	Equivalent Young's modulus (E_{equiv})		
			Experimental (MPa)	Finite Element (MPa)	Difference (%)
0	0.5	124	1284 ± 6.5 %	1267	−1.4
	1	261	1398 ± 6.4 %	1440	3.0
	2	505	1560 ± 5.5 %	1597	2.4
	5	1220	1735 ± 7.8 %	1834	5.7
10	0.5	125	1846 ± 2.2 %	1729	−6.4
	1	248	1942 ± 2.3 %	1949	0.3
	2	505	2181 ± 3.9 %	2173	−0.4
	5	1260	2370 ± 3.0 %	2499	5.5
20	0.5	125	2556 ± 3.5 %	2372	−7.2
	1	256	2781 ± 3.7 %	2657	−4.5
	2	516	2916 ± 4.4 %	2953	1.3
	5	1320	3179 ± 5.6 %	3388	6.6
30	0.5	123	4045 ± 3.0 %	3317	−18.0
	1	245	4220 ± 3.0 %	3682	−12.8
	2	494	4505 ± 3.0 %	4088	−9.3
	5	1240	4823 ± 3.5 %	4637	3.8
40	0.5	120	6458 ± 4.7 %	4836	−25.1
	1	235	6553 ± 4.7 %	5249	−19.9
	2	500	6884 ± 5.2 %	5889	−14.5
	5	1200	7289 ± 6.5 %	6412	−12.0

function of the strain rates.

The deviation in experimental results remains below 8 %, indicating the reliability of results. As seen on Table 4 and on Fig. 14b, the results confirm the influence of the amount of filler particles on the stiffness of nanocomposites. In fact, the experimental and numerical equivalent Young's moduli (E_{equiv}) increase with increasing $BaTiO_3$ filler amount. The stiffness is increased up to 320–400 % (depending on the strain rate) when polymer is filled by 40 v% $BaTiO_3$ compared to neat HDPE. These results also confirm the viscoelastic behavior of the nanocomposite: stiffness increases with increasing strain rate for all samples.

A very good agreement between experimental and numerical results is observed for neat HDPE, 10 v% and 20 v% $BaTiO_3$ filled HDPE indicating that the proposed micromechanical model is representative. For example, for nanoparticle concentration of 20 %, a difference of 4.5 % is found between experimental and numerical results for a crosshead speed of 1 mm/min. For comparison, when a linear elastic model was employed for the polymer [10], this difference reached to 25 % for the same crosshead speed. These observations confirm the effectiveness of the viscoelastic model to better reproduce the behavior of the polymer in the nanocomposite compared to simple linear elastic one.

The discrepancy between experimental and numerical results for higher filler amounts can be attributed to the following potential reasons:

- The filler shape and filler particle distribution play an important role in the mechanical behavior of the composite [39]. In the numerical model, spherical particles are distributed randomly in the polymer matrix without any agglomeration.Experimentally, the formation of filler agglomerates cannot be excluded, since no specific surface modification process was performed on filler particles. Indeed, the X-ray nanotomography in Fig. 2 shows that the filler particles agglomerate in the samples, mainly for high particle concentrations. For 40v% filled HDPE sample, there are less visible individual particles and more agglomerates compared to the 10v%. Numerical simulation has shown that for a given amount of spherical filler, the agglomeration of filler results in a higher stiffness compared to the random distribution [10]. In a similar way, the filler percolation at high filler amount can result in a different experimental stress pathway.
- The interaction between filler particles and polymer matrix is of great consequence on the mechanical properties of nanocomposites. In the numerical model, the interaction between particles and polymer matrix is considered as "perfect contact" without any interphase region. In the literature, the role of an interphase between filler and polymer matrix, with modified polymer properties, has been extensively pointed out [17–19]. But in our numerical model, it is very difficult to take into account the interphase since its properties (thickness, viscoelastic properties …) are unknown and should be considered separately from the polymer matrix. In addition, it is difficult to design manually the interphase around each particle for each random particle distribution. Thus, an interphase region was not considered to simplify the analysis and keep it focused on the viscoelasticity effects.
- From a chemical point of view, the mechanical properties of polymers are in relation with the mobility of chains. In filled polymers, the presence of rigid filler particles can decrease the polymer chain mobility especially for high filler amount where the interparticular distance decreases.

5. Conclusion

The aim of this work was to develop a numerical model able to predict the mechanical behavior of nanocomposites from that of its constituents. Previous research on the subject has shown the limits of model based solely on the elastic behavior of polymers. This work therefore focused on the implementation of a viscoelastic constitutive law in a micromechanical model developed previously. The study was divided into two steps: The first step consisted in defining a viscoelastic model of the neat HDPE based on experimental data. In the second step, this model was implemented into a numerical micromechanical model of the nanocomposite. Particular attention was paid to the correlation between numerical and experimental results.

Tensile tests confirmed viscoelastic behavior of neat HDPE and HDPE filled $BaTiO_3$ nanocomposites: stiffness characterized by the equivalent Young Modulus depends strongly on strain rate. These tests ascertained that a pure elastic model does not permit to accurately simulate the mechanical behavior of this type of material as it does not take into account the time dependence of the mechanical response.

Regarding the determination of the relaxation modulus, the work carried out here has confirmed the impossibility to use only the modulus obtained from a relaxation test: if the load is not applied instantaneously, the measured modulus does not correspond exactly to the relaxation modulus. An approach based on a two-step test has been proposed combining the results of tensile and relaxation tests. Several experiments with different crosshead speeds were performed to determine a master curve of this relaxation modulus. The curve fitting process allowed to define the parameters of a viscoelastic constitutive law based on the generalized Maxwell model. Simulations performed with this model show that it is representative of the mechanical behavior of neat HDPE for different tensile crosshead speeds.

Finally, the implementation of this viscoelastic model in a numerical micromechanical approach showed that it is possible to predict the mechanical behavior of a nanocomposite with a good accuracy for small and intermediate amounts of filler. In particular, it was found that the discrepancy between the numerical and experimental equivalent Young's modulus remains less than 7 % for nanoparticle concentration up to 20 %. For higher amount of filler, further considerations must be taken into account to understand the origin of the differences between experimental and numerical results and improve the model and make it more representative.

In conclusion, this work has highlighted the viscoelastic behavior of neat HDPE and $BaTiO_3$ filled HDPE nanocomposites. The introduction of this viscoelastic behavior into the developed model has greatly improved its representativeness even if some points still need to be further investigated. The strategy developed in this work can be

extended to other filled polymers.

CRediT authorship contribution statement

Jean-Philippe Noyel: Writing – original draft, Supervision, Software, Investigation, Conceptualization. **Ahmad Hajjar:** Writing – original draft, Methodology. **Rafaela Debastiani:** Writing – original draft, Resources, Investigation. **Kevin Antouly:** Resources, Data curation. **Atilla Atli:** Writing – original draft, Supervision, Investigation, Conceptualization.

Declaration of competing interest

The authors declare that they have no known competing financial interests or personal relationships that could have appeared to influence the work reported in this paper.

Data availability

Data will be made available on request.

Acknowledgement

We gratefully thank to our colleague Dr. S. SIMON for her helpful discussion. The laboratory head Dr. P. LOURDIN who allowed us free time to work on this subject is acknowledged. This work was partly carried out with the support of the Karlsruhe Nano Micro Facility (KNMF, ww.knmf.kit.edu), a Helmholtz Research Infrastructure at Karlsruhe Institute of Technology (KIT, www.kit.edu). The Xradia 810 Ultra (nanoCT) core facility was supported (in part) by the 3DMM2O - Cluster of Excellence (EXC-2082/1390761711).

References

[1] T. Tanaka, « barium titanate ceramics and their applications, Bull. Inst. Chem. Res. Kyoto Univ. 32 (2) (1954) 43–53.
[2] J.J. Wang, F.Y. Meng, X.Q. Ma, M.X. Xu, , et al.L.Q. Chen, « Lattice, elastic, polarization, and electrostrictive properties of BaTiO3 from first-principles, J. Appl. Phys. 108 (3) (2010), https://doi.org/10.1063/1.3462441.
[3] X.K. He, L.B. Zeng, Q.S. Wu, L.Y. Zhang, K. Zhu, , et al.Y.L. Liu, Determination of elastic, piezoelectric, and dielectric constants of an R:BaTiO 3 single crystal by Brillouin scattering, Chin. Phys. B 21 (6) (2012), https://doi.org/10.1088/1674-1056/21/6/067801.
[4] H. Yang, et al., High-energy storage performance in BaTiO3-based lead-free multilayer ceramic capacitors, J. Mater. Res. (2020) 1–10, https://doi.org/10.1557/jmr.2020.286.
[5] P. Saini, M. Arora, G. Gupta, B.K. Gupta, V.N. Singh, , et al.V. Choudhary, High permittivity polyaniline-barium titanate nanocomposites with excellent electromagnetic interference shielding response, Nanoscale 5 (10) (2013) 4330–4336, https://doi.org/10.1039/c3nr00634d.
[6] J. Gonzalez-Benito, J. Martinez-Tarifa, M.E. Sepúlveda-García, R.A. Portillo, et G. Gonzalez-Gaitano, Composites based on HDPE filled with BaTiO3 submicrometric particles. Morphology, structure and dielectric properties, Polym. Test. 32 (8) (2013) 1342–1349, https://doi.org/10.1016/j.polymertesting.2013.08.012.
[7] J. Su, , et al.J. Zhang, Comparison of rheological, mechanical, electrical properties of HDPE filled with BaTiO 3 with different polar surface tension, Appl. Surf. Sci. 388 (2016) 531–538, https://doi.org/10.1016/j.apsusc.2015.10.156.
[8] J. Su, , et al.J. Zhang, Preparation and properties of Barium titanate (BaTiO3) reinforced high density polyethylene (HDPE) composites for electronic application, J. Mater. Sci. Mater. Electron. 27 (5) (2016) 4344–4350, https://doi.org/10.1007/s10854-016-4302-2.
[9] S. Basturk, C. Dancer, , et al.T. McNally, Dielectric performance of composites of BaTiO3 and polymers for Capacitor applications under microwave frequency, J. Appl. Polym. Sci. 138 (22) (2021) 50521, https://doi.org/10.1002/app.50521.
[10] A. Atli, J.P. Noyel, A. Hajjar, K. Antouly, E. Lemaire, , et al.S. Simon, Exploring the mechanical performance of BaTiO3 filled HDPE nanocomposites: a comparative study of the experimental and numerical approaches, Polymer 254 (June) (2022), https://doi.org/10.1016/j.polymer.2022.125063.
[11] Y. Zare, , et al.K.Y. Rhee, Development of Hashin-Shtrikman model to determine the roles and properties of interphases in clay/CaCO3/PP ternary nanocomposite, Appl. Clay Sci. 137 (2017) 176–182, https://doi.org/10.1016/j.clay.2016.12.033.
[12] S. Das Lala, S. Sadikbasha, , et al.A.B. Deoghare, Prediction of elastic modulus of polymer composites using Hashin–Shtrikman bound, mean field homogenization and finite element technique, Proc. Inst. Mech. Eng. Part C J. Mech. Eng. Sci. 234 (8) (2020) 1653–1659, https://doi.org/10.1177/0954406219895791.
[13] I. Balac, M. Milovancevic, C.Y. Tang, P.S. Uskokovic, et D.P. Uskokovic, « Estimation of elastic properties of a particulate polymer composite using a face-centered cubic FE model, Mater. Lett. 58 (19) (2004) 2437–2441, https://doi.org/10.1016/j.matlet.2004.02.033.
[14] S. Boutaleb, et al., Micromechanical modelling of the yield stress of polymer-particulate nanocomposites with an inhomogeneous interphase, Procedia Eng. 1 (1) (2009) 217–220, https://doi.org/10.1016/j.proeng.2009.06.051.
[15] H.W. Wang, H.W. Zhou, R.D. Peng, , et al.L. Mishnaevsky, Nanoreinforced polymer composites: 3D FEM modeling with effective interface concept, Compos. Sci. Technol. 71 (7) (2011) 980–988, https://doi.org/10.1016/j.compscitech.2011.03.003.
[16] S.K. Sahu, , et al.P.S.R. Sreekanth, Evaluation of tensile properties of spherical shaped SiC inclusions inside recycled HDPE matrix using FEM based representative volume element approach, Heliyon 9 (3) (2023) e14034, https://doi.org/10.1016/j.heliyon.2023.e14034.
[17] Y. Zare, Study on interfacial properties in polymer blend ternary nanocomposites: role of nanofiller content, Comput. Mater. Sci. 111 (2016) 334–338, https://doi.org/10.1016/j.commatsci.2015.09.053.
[18] J. Amraei, J.E. Jam, B. Arab, , et al.R.D. Firouz-Abadi, Effect of interphase zone on the overall elastic properties of nanoparticle-reinforced polymer nanocomposites, J. Compos. Mater. 53 (9) (2019) 1261–1274, https://doi.org/10.1177/0021998318798443.
[19] M. Zamanian, F. Ashenai Ghasemi, , et al.M. Mortezaei, An efficient nanoscale representative volume element simulation including graded interphase for tensile behavior of epoxy/silica nanocomposites, J. Appl. Polym. Sci. 138 (45) (2021) 1–10, https://doi.org/10.1002/app.51332.
[20] X. Xu, C. Koomson, M. Doddamani, R.K. Behera, et N. Gupta, Extracting elastic modulus at different strain rates and temperatures from dynamic mechanical analysis data: a study on nanocomposites, Composites, Part B 159 (October 2018) (2019) 346–354, https://doi.org/10.1016/j.compositesb.2018.10.015.
[21] K. Yang, H. Cai, W. Yi, Q. Zhang, , et al.K. Zhao, « Static viscoelasticity of biomass polyethylene composites, Results Phys 7 (2017) 2568–2574, https://doi.org/10.1016/j.rinp.2017.05.029.
[22] S. Siengchin, , et al.V. Rungsardthong, HDPE reinforced with nanoparticle, natural and animal fibers: morphology, thermal, mechanical, stress relaxation, water absorption and impact properties, J. Thermoplast. Compos. Mater. 26 (8) (2013) 1025–1040, https://doi.org/10.1177/0892705712454867.
[23] X. Shi, M.K. Hassanzadeh-Aghdam, , et al.R. Ansari, Viscoelastic analysis of silica nanoparticle-polymer nanocomposites, Composites, Part B 158 (July 2018) (2019) 169–178, https://doi.org/10.1016/j.compositesb.2018.09.084.
[24] Y. Chen, Z. Zhao, Z. Guo, , et al.Y. Li, Micromechanical model of linear viscoelastic particle-reinforced composites with interphase, Appl. Math. Model. 97 (2021) 308–321, https://doi.org/10.1016/j.apm.2021.03.056.
[25] C.F. Popelar, C.H. Popelar, , et al.V.H. Kenner, Viscoelastic material characterization and modeling for polyethylene, Polym. Eng. Sci. 30 (10) (1990) 577–586, https://doi.org/10.1002/pen.760301004.
[26] C. Zhang, , et al.I.A.N.D. Moore, Nonlinear mechanical response of high density polyethylene. Part I: experimental investigation and ModeI EvaIuation, Polym. Eng. Sci. 37 (2) (1997) 404–413.
[27] Amjadi et Fatemi, Tensile behavior of high-density polyethylene including the effects of processing technique, Polymers 12 (2020) 1857, https://doi.org/10.3390/polym12091857.
[28] Q. Mao, B. Su, R. Ma, , et al.Z. Li, Investigation of tensile creep behavior for high-density polyethylene (Hdpe) via experiments and mathematical model, Materials 14 (20) (2021), https://doi.org/10.3390/ma14206188.
[29] T.C. da Costa-Haveroth, et al., Aspects on viscoelasticity modeling of HDPE using fractional derivatives: interpolation procedures and efficient numerical scheme, Mech. Adv. Mater. Struct. 29 (25) (2022) 4343–4358, https://doi.org/10.1080/15376494.2021.1928345.
[30] N. Dusunceli, , et al.O.U. Colak, The effects of manufacturing techniques on viscoelastic and viscoplastic behavior of high density polyethylene (HDPE), Mater. Des. 29 (6) (2008) 1117–1124, https://doi.org/10.1016/j.matdes.2007.06.003.
[31] A. Stankiewicz, Identification of relaxation modulus of viscoelastic materials from non-ideal ramp-test histories – problem and method, Teka Comm. Mot. Power Ind. Agric. 13 (1) (2013) 177–184.
[32] J. Sorvari, , et al.M. Malinen, On the direct estimation of creep and relaxation functions, Mech. Time-Dependent Mater. 11 (2) (2007) 143–157, https://doi.org/10.1007/s11043-007-9038-1.
[33] R. Elleuch, , et al.W. Taktak, Viscoelastic behavior of HDPE polymer using tensile and compressive loading, J. Mater. Eng. Perform. 15 (1) (2006) 111–116, https://doi.org/10.1361/105994906X83475.
[34] A. Flory, , et al.G.B. Mckenna, Finite step rate corrections in stress relaxation experiments: a comparison of two methods, Mech. Time-Dependent Mater. 8 (1) (2004) 17–37, https://doi.org/10.1023/B:MTDM.0000027681.86865.4a.
[35] I.M. Ward, , et al.J. Sweeney, Mechanical Properties of Solid Polymers, 2013, https://doi.org/10.3139/9783446402447.001. Wiley&Sons.
[36] M.T. Shaw, , et al.W.J. MacKnight, Introduction to Polymer Viscoelasticity, wiley&Sons, 2005.
[37] A.R. Shahani, H. Shooshtar, A. Karbasian, , et al.M.M. Karimi, Evaluation of different methods of relaxation modulus extraction for linear viscoelastic materials

from ramp-constant strain experiments, Proc. Inst. Mech. Eng. Part C J. Mech. Eng. Sci. 233 (9) (2019) 3155–3169, https://doi.org/10.1177/0954406218802599.
[38] S. Lee, , et al.W.G. Knauss, Note on the determination of relaxation and creep data from ramp tests, Mech. Time-Dependent Mater. 4 (1) (2000) 1–7, https://doi.org/10.1023/A:1009827622426.
[39] C. DeArmitt, et al., Hancok michael, « filled thermoplastics, in: R.N. Rothon (Ed.), Particulate-Filled Polymer Composites, N° August, Rapra Technology Limited, 2003, p. 544.